Session 12: Research Track

Towards characterizing green roof vegetation using color-infrared and thermal sensors

Deon van der Merwe, Lee R. Skabelund, Ajay Sharda, Pamela Blackmore, Dale Bremer
Kansas State University: KSU-VetMed/KSU- LARCP/KSU-BAE/KSU-LARCP/KSU-HORT

ABSTRACT

Researchers at Kansas State University (KSU) initiated studies of vegetation growing on the KSU Memorial Stadium green roofs (MS-GRs) after these combined 0.40-hectare green roofs were seeded and planted with 30 native species. On-the-ground vegetation assessment was aided utilizing aerial sensors to provide imagery that helps reveal vegetation cover and growth/vigor. Thermal (FLIR VUE PRO 640) and color-infrared (CIR; modified Canon S100) sensors were used on a small unmanned aircraft system (sUAS; 3DR Iris+) on separate flights—completed midday on July 5, 2016. Images were collected from 50 meters above the MS-GRs, with 80% overlap front-to-back and side-to-side. Surface elevation models and orthomosaics were constructed using a surface-from-motion method (Agisoft-Photoscan-Pro), with reflectance values averaged from all contributing images, and models georeferenced using ground control points. Thermal orthomosaics were calibrated based on a series of ground targets with known surface temperatures, and were transformed into temperature maps. CIR orthomosaics were transformed into normalized difference vegetation index (NDVI) maps. 2016 results indicate that green roof surface temperature and NDVI values are correlated with vegetative cover. It was found that sUAS-based sensors provide viable, efficient data collection, offering a potential practical application for vegetation characterization on green roof installations. Quantitative analysis and correlation between plant characteristics and high spatial resolution remotely sensed data is required to develop and realize the potential of this emerging technology. July 2017 sUAS flights collected additional data.

INTRODUCTION

Over 770,000 unmanned aircraft systems (UAS) have been registered with the Federal Aviation Administration in the United States (Yurieff, 2017). The diversity of UAS applications in many arenas continues to expand with numerous helpful uses being realized. UAS are becoming increasingly popular for remote sensing because they are a relatively inexpensive way to frequently obtain a variety of data at variable spatial resolutions (Tang & Shao, 2015). UAS have been used in many fields including, but not limited to, military support, forestry (both for forest fire management and vegetation monitoring) wildlife management, observation and remote sensing—such as surveying and mapping, the energy sector (for such tasks as monitoring infrastructure), and agriculture (Colomina & Molina, 2014).

One important area where UAS are being used is in crop management. This application involves collecting high spatial resolution, multispectral imagery obtained by sensors mounted on UAS to predict crop productivity, detect weeds, identify nutrient deficiencies and diseases, and inform about overall crop condition (Mazur, 2016). Similar methods, based on low altitude CIR aerial imagery, have also been applied successfully to estimate biomass in tallgrass prairie ecosystems (Wang, Price, Van der Merwe, An & Wang, 2014). High spatial resolution data, at the scale of local fields or experiments, can be acquired inexpensively and frequently, in comparison to the use of satellite imagery, which was previously the preferred method for obtaining this information (Berni, Zarco-Tejada, Suárez, & Fereres, 2009; Mazur, 2016). Successful use of these methods in agricultural fields suggests that similar methods have the potential for successful deployment in urban settings with urban vegetation types such as green roof installations.

This article describes the methods used in one such scenario: using an UAS to evaluate green roof vegetation for a created prairie-like system. Data gathered by means of UAS-mounted CIR and infrared thermography (IRT) sensors were used to increase understanding of spatial patterns in vegetative cover, growth vigor, surface elevation, and surface temperatures of two green roof installations of approximately 0.20 hectares each.

GREEN ROOF ASSEMBLY, VEGETATION, IRRIGATION, AND MAINTENANCE

On the KSU campus in Manhattan, Kansas, the two wings of the World War I Memorial Stadium were retrofitted with two green roofs, replacing a substantial portion of the stadium seating by filling in stair-step seating with insulation and then adding green roof components (Figure 1a).

Figure 1a: West Memorial Stadium Green Roof Implementation (L. Skabelund, May 2014 to June 2015)

The vegetation selected for these sloped (approximately 20º or 36%) green roofs was a mixture of tallgrass prairie species native to the area. Each green roof has different substrates: both are sand-based, but the East Memorial Stadium Green Roof (EMS-GR) includes expanded shale to lighten the structural load. Vegetation on each roof also differs, with the EMS-GR having fewer native grasses due to these not being included in the seed mix. Native species seeded and/or planted as live plants or plugs are listed in Appendix A: Table 1. (For more about MS-GR components and initial 2016-2017 monitoring efforts refer to our KSU MS-GR monitoring paper—Cities Alive 2017, Session 22: Research Track.)

The West Memorial Stadium Green Roof (WMS-GR) was seeded on June 23, 2015, and July 2, 2015, then planted on July 2, 2015. The EMS-GR was seeded and planted approximately nine months later—with seeding on March 18, 2016, and planting initiated on April 7, 2016. Live plants (both grasses and wildflowers) were planted in the middle of the geo-web cells, roughly 30 cm apart. (Refer to Figure 1b for an image taken during planting of the EMS-GR.)

Figure 1b: East Memorial Stadium Green Roof Planting Work (L. Skabelund, 7 April 2016)

The vegetation on each green roof is irrigated (using Hunter I-20-12 rotor spray heads at a rate of approximately 1 cm per hour), fertilized (using an organic fertilizer sprayed onto each roof several times a year), and clipped and weeded and/or trimmed/weed-whacked (several times a year, as needed; with trimming to 20-30 cm occurring in mid-July and mid-September 2016 on the EMS-GR). Weeding and clipping undertaken on the two MS-GRs occurred during the spring and early summer of 2016 prior to the July 5, 2016, UAS flights with the goal of reducing agricultural weeds and tree seedlings (mid-May to late-June on both MS-GRs).

The aim of small unmanned aircraft system (sUAS) flights is to increase the amount and quality of available information about vegetation dynamics on these green roofs, with the goal of using such information to enhance green roof management (namely irrigation, fertilization, and weeding/clipping practices).

While other on-site vegetation studies were ongoing (including plant identification walkabouts and plant species identification along eight transects on each roof), it was decided that the use of an sUAS could help characterize and better understand the overall patterns of vegetative growth, vegetative changes, and thermal temperatures on each roof.

Given that patterns and changes in vegetation coverage require ongoing studies, our desire is to complete species identification along transects for at least five years, and to use sUAS imagery to help track mid-growing season changes year-to-year during that same five-year period. The annual identification of plant species along the eight transects and across each green roof helps researchers understand changes in species dominance and richness.

On July 5, 2017, sUAS flights provided additional CIR, IRT, and true-color imagery which can be used to support investigations of vegetative change on each green roof. Naturally, the ability to complete these green roof monitoring activities over the next three years (along with supporting analysis work) will depend on securing sufficient funding, personnel, and expertise to complete these tasks.

METHODS

IRT (FLIR VUE PRO 640 R with 13 mm lens) and CIR (modified Canon S100; MaxMax.com) sensors were used on a small unmanned aircraft system (sUAS; 3DR Iris+; see Figure 2a) on separate flights—completed between 11am and 12 noon CDT on July 5, 2016. Images were collected from 50 meters above the MS-GRs, with 80% overlap front-to-back and side-to-side. A flight altitude of 50 meters was chosen because it provided an optimal compromise between spatial resolution and flight efficiency. It was appropriate for the flight duration of the sUAS used and the pixel density of the sensors, which provided adequate image resolution to differentiate objects such as temperature targets at a resolution needed to determine target reflectance without the use of pixels influenced by target edges.

Flight operations were conducted by a licensed pilot (Figure 2b) using a registered aircraft under the Federal Aviation Administration Small Unmanned Aircraft Rule (14 CFR Part 107).

Figure 2: Preparations to fly the sUAS over the Memorial Stadium Green Roofs on July 5, 2016.
2a – sUAS being kept cool with a small covering pre-flight, with the EMS-GR in the background.
2b – sUAS pilot Deon van der Merwe finishing flight-plan commands on his laptop computer.

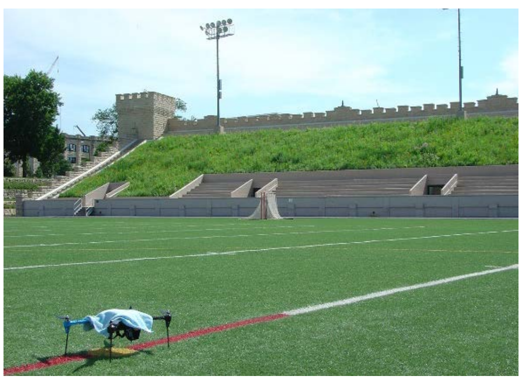
2a


2b

Surface elevation models and orthomosaics were constructed using a surface from motion method (Agisoft-Photoscan-Pro), with reflectance values averaged from all contributing images. An average of 7 images (range 5-8) contributed to each reflectance value in the area of interest), and models were georeferenced using a sub-2 cm GNSS RTK receiver programmed to output data at 10 Hz (GR5 rover and GR5 base connected through an FH915 plus radio modem; Topcon Positioning Systems, Inc., Livermore, CA, USA). Georeferenced orthomosaics were displayed and analyzed in a geographical information system environment (ESRI ArcGIS).

Thermal orthomosaics, with a spatial resolution of 10 cm, were calibrated based on a series of ground targets with known surface temperatures, including 3' by 2' wood panels painted white, grey, and black, and invariant surfaces in the area of interest such as concrete and athletic track surfaces, for a total of 13 ground targets in each of the green roof installations. The ground target temperatures were determined using a hand-held infrared thermal sensor (Fluke 561), with emissivity set to 0.95. Linear regression models were used to transform 8-bit thermal orthomosaic pixel values into temperature values, displayed as temperature maps (Appendix B, Figs. 5 & 6). The linear regression models were T = 0.3196(X) + 29.515 and T = 0.3555(X) + 24.833, with R^2-values of 0.9543 and 0.9235, respectively, for the West installation and the East installation, where T is surface temperature (°C); and X is 8-bit pixel intensity value.

Although the surface temperatures used for model calibration were estimated at the time of flight, the regression model should not be interpreted as a reliable indication of the absolute or actual temperature because surface temperatures can vary over the span of minutes due to changes in sunlight intensity and angle, and wind effects. The chosen emissivity value is also a potential contributor to error, due to the complexity and variety of surfaces in the study area that are likely to have unique emissivity values depending on the specific characteristics of each surface. The regression model should be viewed as an estimate of relative surface temperatures during the time of flight. The interpretation of temperature data is, however, based on relative temperatures (the temperatures of objects relative to a reference object or series of objects), and relative temperatures are therefore useful despite the potential for absolute error (the difference between the measured or inferred value of a quantity and its actual value).

CIR orthomosaics (Appendix B, Figures 4 & 5), with a spatial resolution of 1.6 cm, were transformed into normalized difference vegetation index (NDVI) maps (Appendix B, Figures 8 & 9) using the following model: NDVI = (Nir -VIS)/(Nir + VIS), where Nir is near infrared (*c.* 690-780 nm) and VIS is visible light (*c*. 450-550 nm). Due to the use of broad bands from a converted consumer camera to provide Nir and VIS data, and specifically using the camera's green channel to provide the visible light band, the resulting NDVI variant was referred to as GNDVI to differentiate it from traditional NDVI maps derived from multispectral sensors.

The use of a green band and Nir band for producing an NDVI in this study is unusual compared to the bulk of the NDVI literature that reports NDVI based on red and Nir bands. The use of the green band has, however, become popular in recent years due to the increasing use of low altitude sUAS fitted with modified consumer cameras that detect blue, green and Nir bands. The theoretical basis for using the green band is that plants utilize the entire visible spectrum for photosynthesis (McCree, 1972), and the green band can therefore be used instead of a red band to produce an NDVI that is correlated with photosynthetic potential.

It is important to consider the sources and significance of spatial errors when working at the ultra-high spatial resolution used in this project. Two types of error need to be considered: relative error and absolute error. The potential for relative positional error of objects in orthomosaics generated using the surface from motion method is influenced by the spatial resolution of the imagery. In the horizontal plane, a potential relative positional accuracy of up to two pixel widths is typical, therefore up to 20 cm for the thermal orthomosaic, and up to 3 cm for the CIR orthomosaic, respectively. The absolute error is controlled by the use of ground control points (GCPs). The error therefore depends on the quality and distribution of the GCPs, with the best accuracy being the same as the accuracy of the GCPs. Errors can be generated in the modeling process, and can be propagated through areas where GCPs are absent or sparse. In this study, a potential absolute error control of <2 cm was achieved by using an RTK system. True absolute error could, however, be larger, particularly in areas of the orthomosaics not in close proximity to GCPs. The impact of spatial location errors in this type of ultra-high resolution aerial imagery is, however, of less importance compared to similar error considerations in high altitude aerial imagery. Objects such as plants and clusters of plants can be observed and recognized due to their unique spatial patterns, textures and relative positions. Image-derived values can therefore be related directly to objects on the ground.

RESULTS

Thermal maps are represented in Figures 6 and 7. Surface temperatures in the WMS-GR installation ranged from 31.8 °C to 66.9 °C, with a strong trend towards higher temperatures at the higher end of the slope. Surface temperatures in the EMS-GR installation were generally lower, ranging from 25.2 °C to 61.7 °C, and did not contain a consistent slope-related trend. Lower temperatures on the EMS-GR were likely caused by a combination of less direct solar irradiance during the preceding morning hours (due to the west-facing slope of the EMS-GR versus the east-facing slope of the WMS-GR roof), differences in vegetation composition (see Figure 2), which may have resulted in greater transpirational cooling on the EMS-GR than the WMS-GR, and the cooling effects of mid-morning irrigation on the EMS-GR (as opposed to early morning irrigation on the WMS-GR).

GNDVI maps are represented in Figures 8 and 9. Spatial patterns in GNDVI values correlated with spatial patterns in surface temperature, with lower surface temperatures associated with higher GNDVI values. These variations were also correlated with variations in plant biomass assessed subjectively from ground level, where higher biomass was correlated with lower surface temperatures and higher GNDVI values. These observations strongly suggested relationships between biomass and image-derived parameters. These relationships need to be confirmed and quantified in future studies.

Complex spatial variations were overlaid onto the underlying biomass-related trends. These variations appeared to be correlated with plant community structure, assessed subjectively at ground level (see Figure 3). Spatially detailed assessments of plant community structure are needed to quantify these relationships.

Figure 3: June 29, 2016 image of WMS-GR paired with two sUAS images taken on July 5, 2016.
3a – notice the relationship between higher, drier portions of the WMS green roof, cooler temperatures, and increasing biomass near the mid-elevation portion of the WMS-GR. Note, however, that these relationships (observed but not quantified) are not one-to-one.
3b – sUAS thermal image shows increasing soil moisture at lower elevations of the WMS-GR.
3c – sUAS-derived NDVI image clearly reveals browned out biomass at top of the WMS-GR.


3a

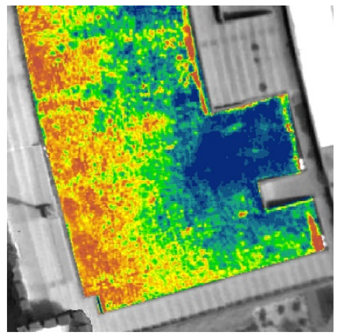
3b

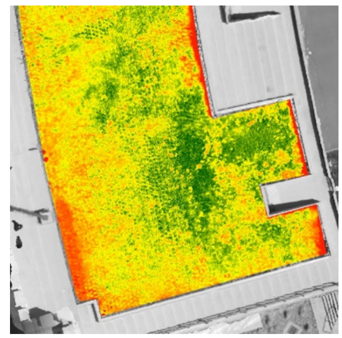
3c

CONCLUSIONS

The observed correlations between surface temperature and biomass confirmed the expectations that surface temperatures are affected by plant cover due to the cooling effects of evapotranspiration. This effect is expected to be more pronounced under high environmental temperature conditions, and when plants have adequate water resources. Clearly there is great complexity which cannot be fully sorted out without much more in-depth study and integrated soil moisture, surface and subsurface temperature, and vegetation analysis.

Quantitative analysis and correlation between plant characteristics and high spatial resolution remotely sensed data is required to develop and realize the potential of this emerging technology. Vegetation analysis should include plant community composition, and quantitative assessment of plant biomass, structure, and phenology. Although this is beyond research budget for this project, what we hope to ascertain are the key drivers and important interrelationships via ongoing study on the roof and use of UAS imagery.

Thermal and NDVI orthomosaics derived from sensors mounted on an sUAS provided excellent and efficient overviews of the green roof installations, making it possible to observe complex spatial patterns and associations. It also provided excellent baseline data that will enable the detection and quantification of changes over time, and will help to appreciate the extent and significance of vegetation changes over time. However, these data should not be utilized in isolation, and should be validated, carefully analyzed, and interpreted in conjunction with ground-based observations.

REFERENCES

Berni, J. A. J., Zarco-Tejada, P. J., Suárez, L., & Fereres, E. (2009). Thermal and Narrowband Multispectral Remote Sensing for Vegetation Monitoring From an Unmanned Aerial Vehicle. *IEEE TRANSACTIONS ON GEOSCIENCE AND REMOTE SENSING*. https://doi.org/r 10.1109/TGRS.2008.2010457

Colomina, I., & Molina, P. (2014). Unmanned aerial systems for photogrammetry and remote sensing: A review. *ISPRS Journal of Photogrammetry and Remote Sensing*, *92*, 79–97. https://doi.org/10.1016/j.isprsjprs.2014.02.013

Mazur, M. (2016). Six Ways Drones Are Revolutionizing Agriculture - MIT Technology Review. Retrieved May 31, 2017, from https://www.technologyreview.com/s/601935/six-ways-drones-are-revolutionizing-agriculture/

McCree, K. J. (1972) The action spectrum, absorptance and quantum yield of photosynthesis in crop plants. *Agricultural Meteorology*. 9, 191-216. http://www.sciencedirect.com/science/article/pii/0002157171900227

Tang, L., & Shao, G. (2015). Drone remote sensing for forestry research and practices. *Journal of Forestry Research*, *26*(4), 791–797. Retrieved from https://www.researchgate.net/profile/Lina_Tang2/publication/283655699_Drone_remote_sensing_for_forestry_research_and_practices/links/5672302108aecc73dc09c776.pdf

Yurieff, K. (2017). U.S. drone registrations skyrocket to 770,000 - Mar. 28, 2017. Retrieved May 31, 2017, from http://money.cnn.com/2017/03/28/technology/us-drone-registrations/

Wang, C., Price K. P., Van der Merwe, D., An, N., Wang, H. (2014). Modeling above-ground biomass in tallgrass prairie using ultra-high spatial resolution sUAS imagery. *Photogrammetric Engineering & Remote Sensing,* 80(12), 1151-1159. http://www.asprs.org/a/publications/pers/2014journals/PERS_December_2014/HTML/files/assets/basic-html/index.html#1151

APPENDIX

Appendix A: Table 1. Taxa (Plant Species) Specified for the Memorial Stadium Green Roofs in 2015 and 2016 (as synthesized from Applied Ecological Services Taylor Creek Nurseries and Blueville Nursery Inc. documentation), with MS-GR seed notes.

Plant Species	Seed or Live Plant/Plug	Green Roof
Allium stellatum	Seed	East and West
Baptisia australis	Seed	East and West
Camassia scilloides	Seed	East and West
Ratibida columnifera	Seed	East and West
Tradescantia ohiensis	Seed	East
Symphyotrichum ericoides	Seed	East and West
Artemisia ludoviciana	Seed	East and West
Oligoneuron rigida	Seed	East and West
Achillea millefolium	Live Plant	East and West
Dalea purpurea	Live Plant	East and West
Echinacea pallida	Live Plant	East and West
Liatris aspera	Live Plant	East and West
Liatris pycnostachya	Live Plant	East and West
Monarda fistulosa	Live Plant	East and West
Penstemon cobaea	Live Plant	East and West
Penstemon digitalis	Live Plant	East and West
Salvia azurea	Live Plant	East and West
Schizachyrium scoparium	Live Plant	East and West
Sorghastrum nutans	Live Plant	East and West
Sporobolus heterolepis	Live Plant	East and West
Symphyotrichum novae-angliae	Live Plant	East and West
Asclepias tuberosa	Live Plant	West
Scutellaria leonardii	Seed	West
Ratibida pinnata	Seed	West
Carex glauca	Seed	West
Symphyotrichum sericeum	Seed	West
Tradescantia occidentalis	Seed	West
Bouteloua curtipendula	Seed	West
Bouteloua gracilis	Seed	West
Bouteloua hirsuta	Seed	West

MS-GR Seeding Notes:

WMS-GR - 6 pounds of native grasses and sedges seed, plus 27 pounds of wildflower seed (2.5 pounds per species) for a total of 33 pounds (~15 kg) of prairie seed.

EMS-GR - only wildflower seed added: 2.5 pounds of seed for each wildflower species, for a total of 20 pounds (~9 kg).

Appendix B: Imagery obtained using an sUAS July 5, 2016 (Figure 4).

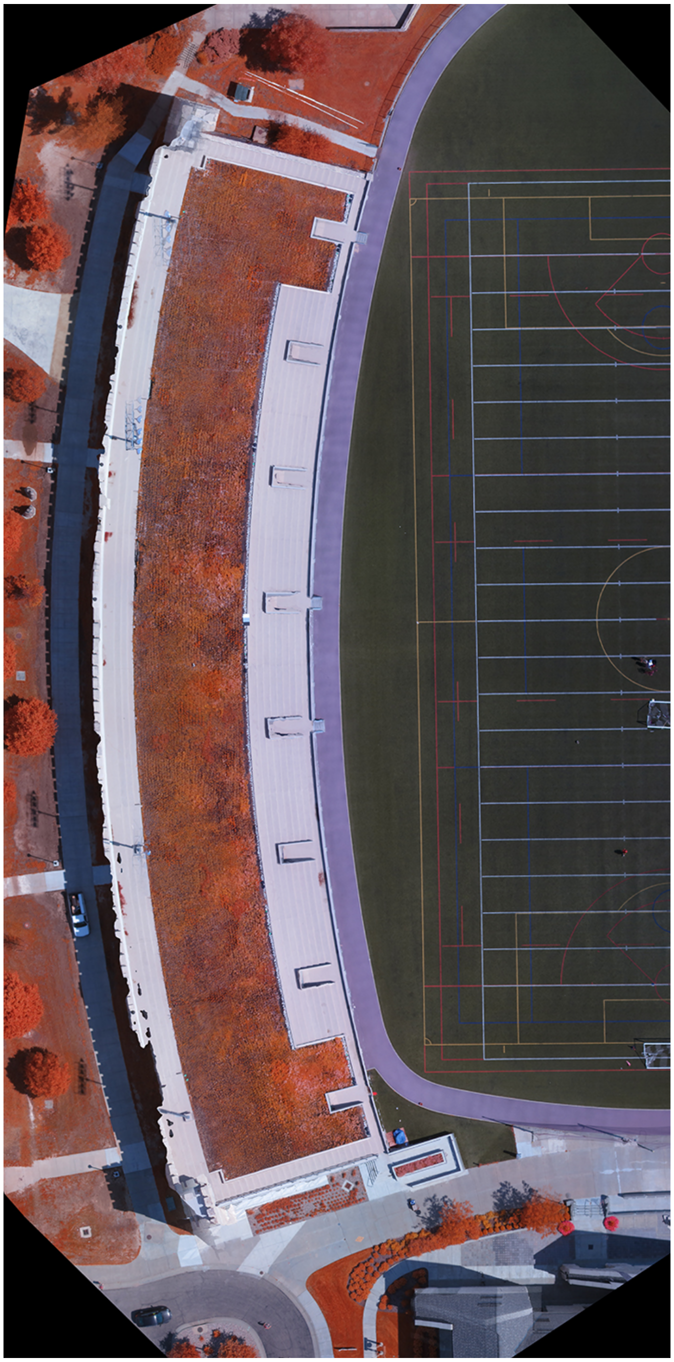

Figure 4: Color-infrared map with 1.6 cm spatial resolution of WMS-GR vegetation, generated from aerial images collected on July 5, 2016.

Appendix B: Imagery obtained using an sUAS July 5, 2016 (Figure 5).

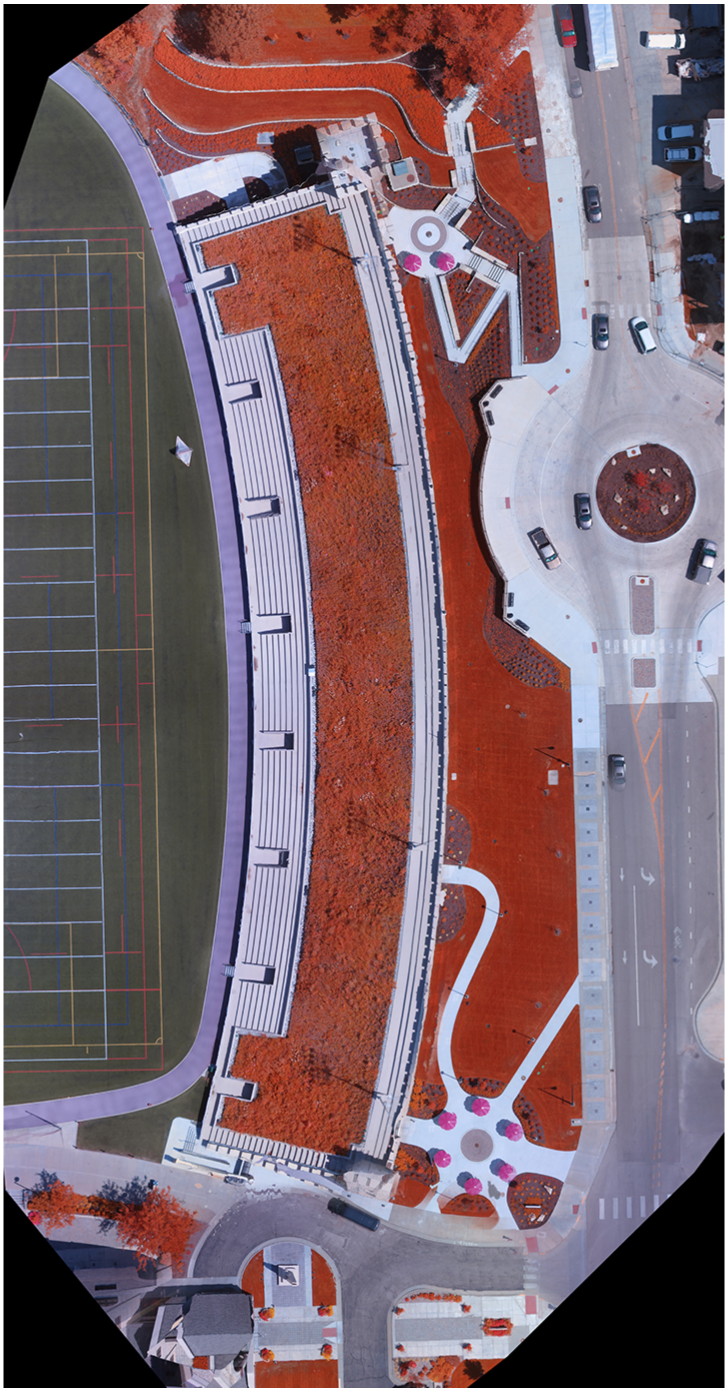

Figure 5: Color-infrared map with 1.6 cm spatial resolution of EMS-GR vegetation, generated from aerial images collected on July 5, 2016.

Appendix B: Imagery obtained using an sUAS July 5, 2016 (Figure 6).

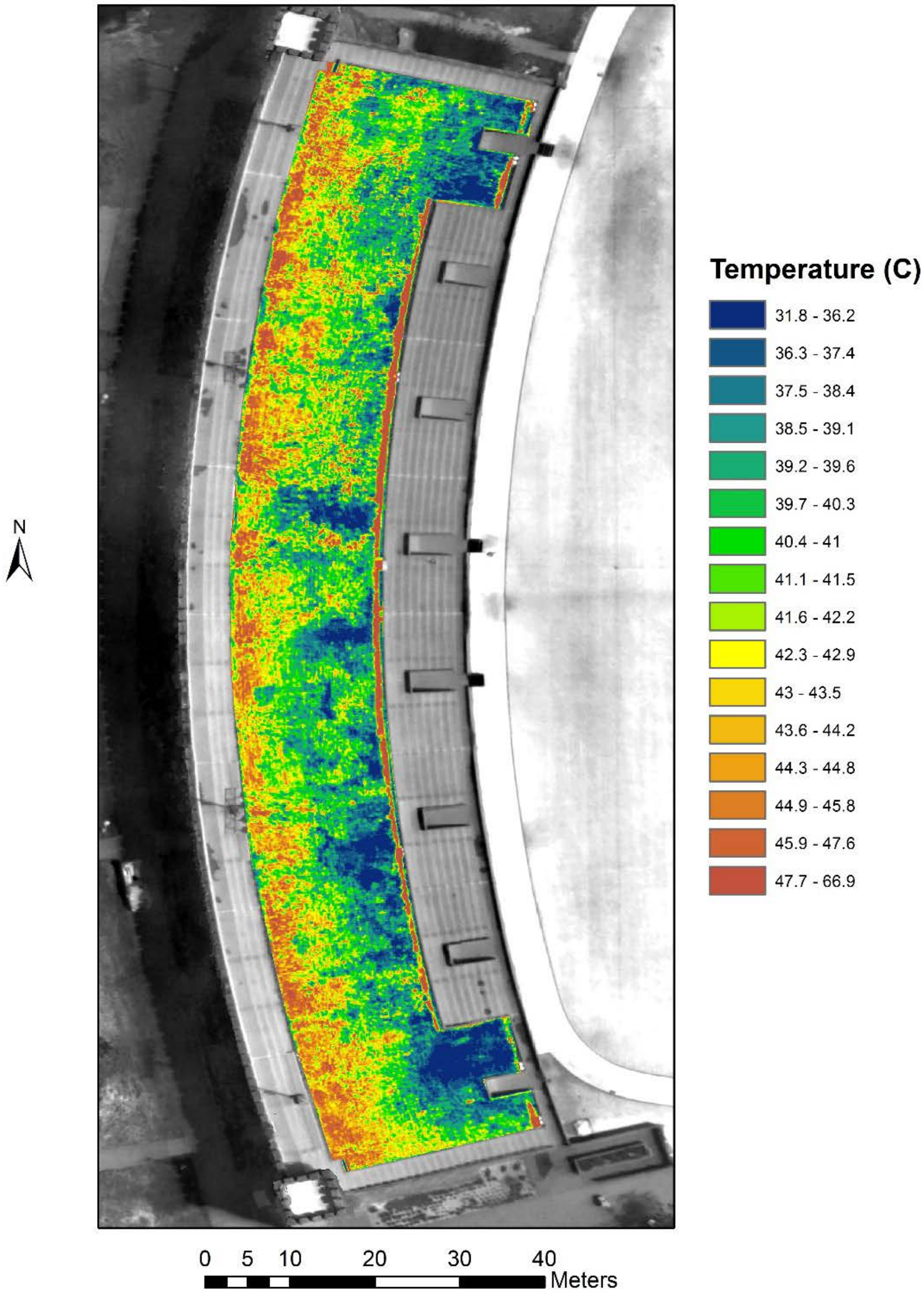

Figure 6: Thermal map with 10 cm spatial resolution of the WMS-GR installation, generated from thermal images collected on July 5, 2016.

Appendix B: Imagery obtained using an sUAS July 5, 2016 (Figure 7).

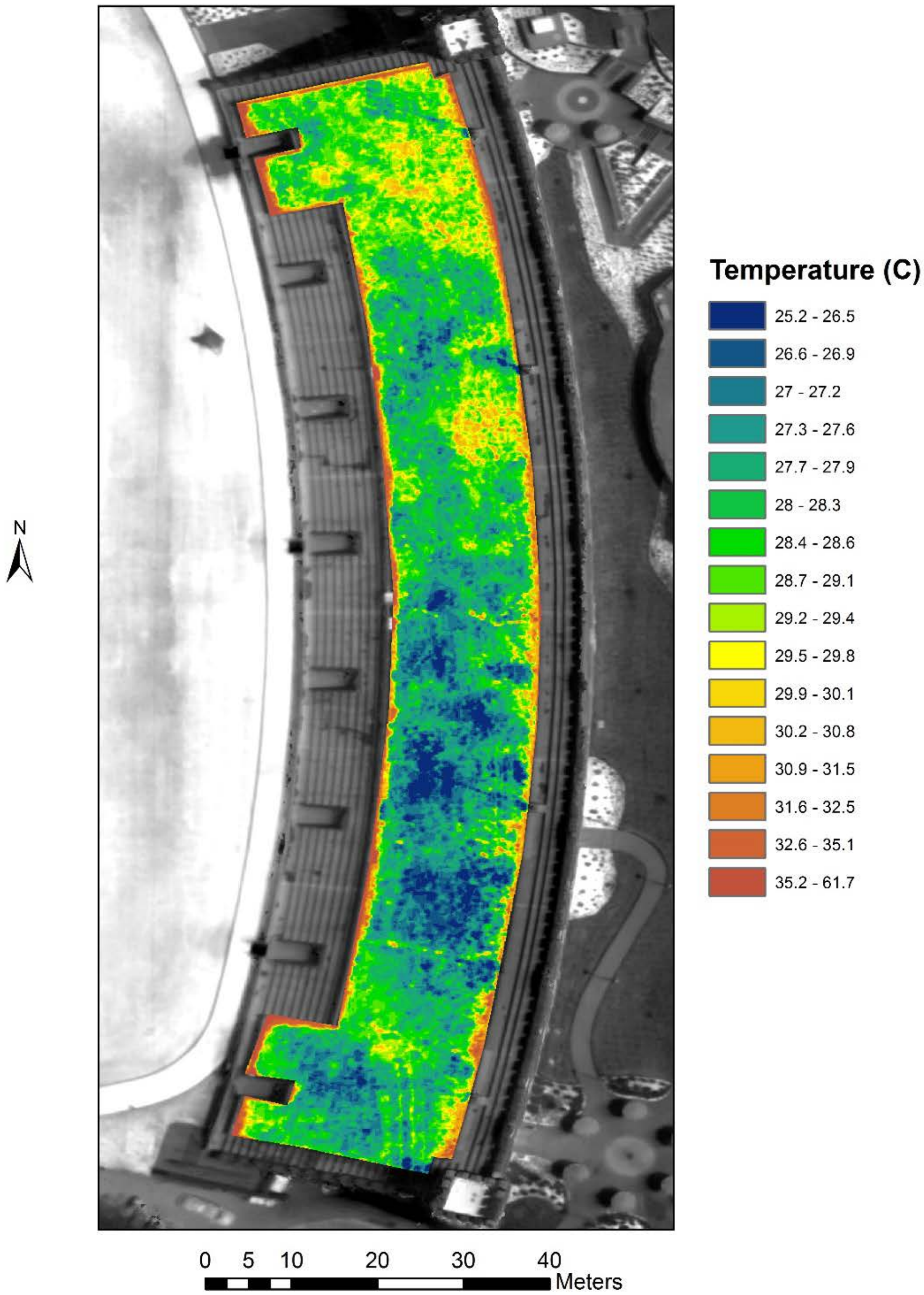

Figure 7: Thermal map with 10 cm spatial resolution of the EMS-GR installation, generated from thermal images collected on July 5, 2016.

Appendix B: Imagery obtained using an sUAS July 5, 2016 (Figure 8).

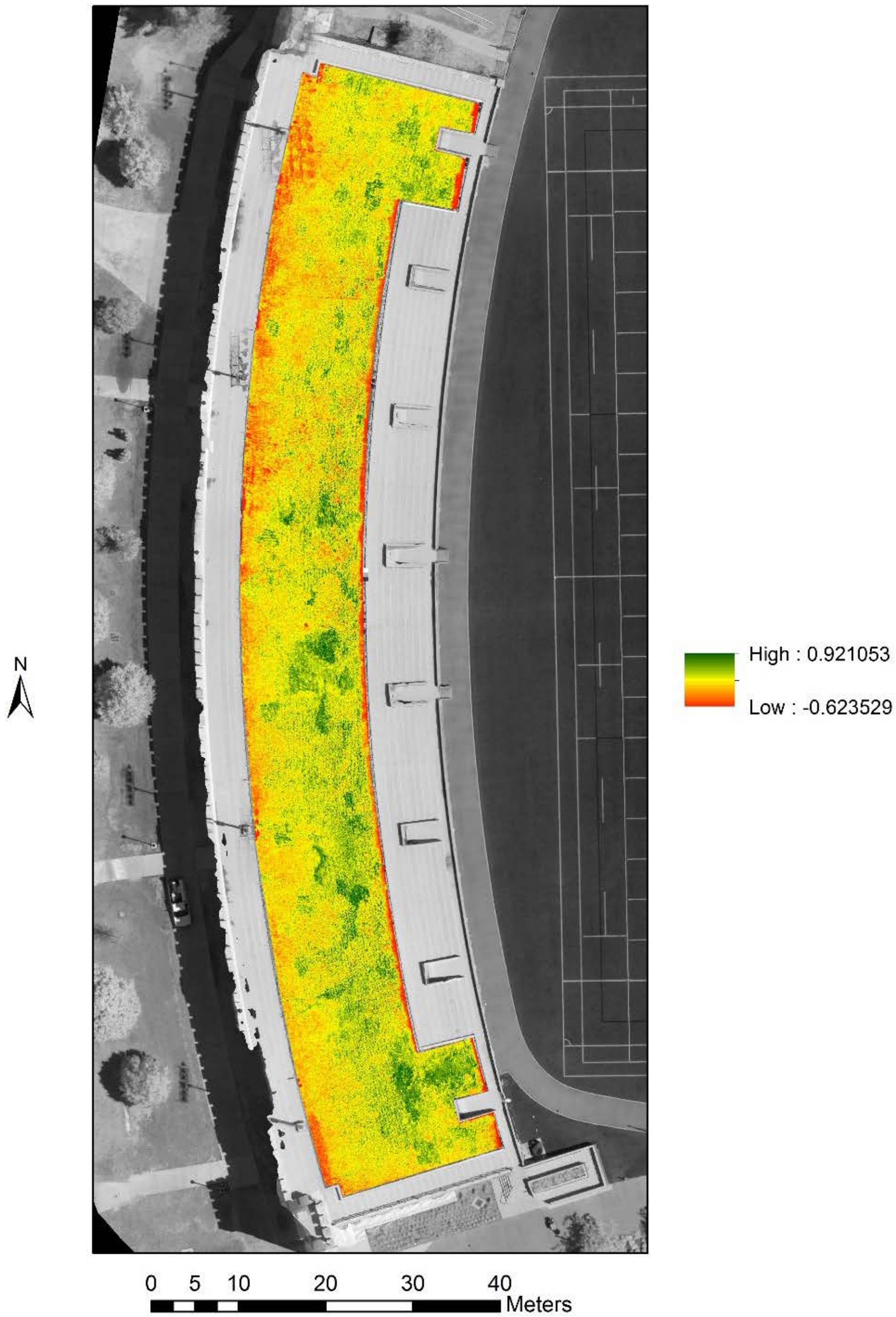

Figure 8: NDVI map with 1.6 cm spatial resolution of the WMS-GR installation, generated from color-infrared images collected on July 5, 2016.

Appendix B: Imagery obtained using an sUAS July 5, 2016 (Figure 9).

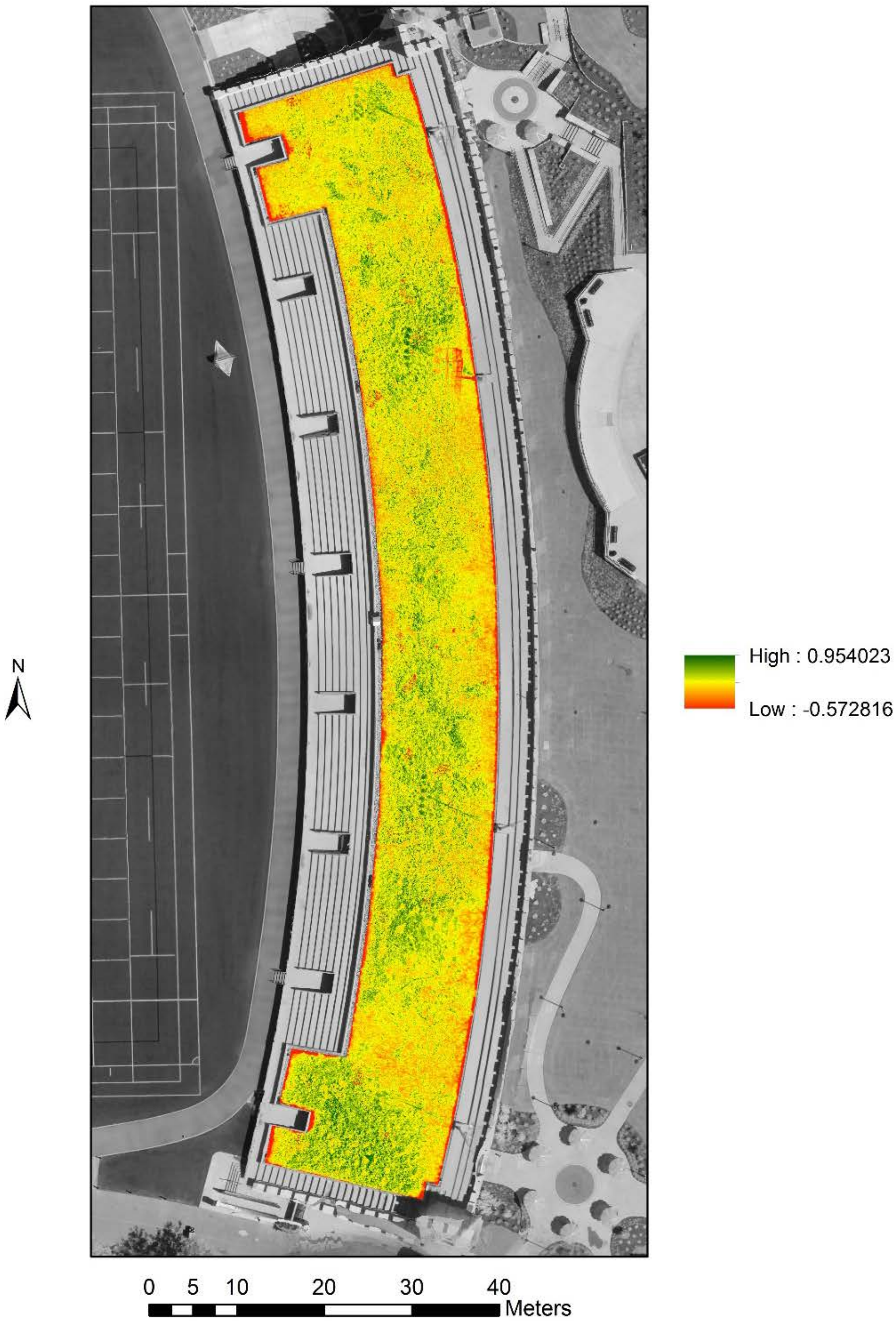

Figure 9: NDVI map with 1.6 cm spatial resolution of the EMS-GR installation, generated from color-infrared images collected on July 5, 2016.